Acta Pharmaceutica Sinica B 2023;13(9):3744–3755

Chinese Pharmaceutical Association
Institute of Materia Medica, Chinese Academy of Medical Sciences

Acta Pharmaceutica Sinica B

www.elsevier.com/locate/apsb
www.sciencedirect.com

ORIGINAL ARTICLE

Translocation of IGF-1R in endoplasmic reticulum enhances SERCA2 activity to trigger Ca^{2+}_{ER} perturbation in hepatocellular carcinoma

Yanan Li[a], Keqin Li[b], Ting Pan[a], Qiaobo Xie[b], Yuyao Cheng[a], Xinfeng Wu[b], Rui Xu[b], Xiaohui Liu[b], Li Liu[c], Jiangming Gao[c], Wenmin Yuan[c], Xianjun Qu[b,*], Shuxiang Cui[a,*]

[a]*Department of Toxicology and Sanitary Chemistry, Beijing Key Laboratory of Environmental Toxicology, School of Public Health, Capital Medical University, Beijing 100069, China*
[b]*Department of Pharmacology, School of Basic Medical Sciences, Capital Medical University, Beijing 100069, China*
[c]*Department of Pharmacology, Marine Biomedical Research Institute of Qingdao, Qingdao 266071, China*

Received 17 January 2023; received in revised form 5 May 2023; accepted 6 May 2023

KEY WORDS

IGF-1R;
HCC;
Endoplasmic reticulum (ER);
SERCA2;
Ca^{2+}_{ER} perturbation;
βarrestin-2 (β-arr2);
$SERCA2^{Y990}$;
Thapsigargin

Abstract The well-known insulin-like growth factor 1 (IGF1)/IGF-1 receptor (IGF-1R) signaling pathway is overexpressed in many tumors, and is thus an attractive target for cancer treatment. However, results have often been disappointing due to crosstalk with other signals. Here, we report that IGF-1R signaling stimulates the growth of hepatocellular carcinoma (HCC) cells through the translocation of IGF-1R into the ER to enhance sarco-endoplasmic reticulum calcium ATPase 2 (SERCA2) activity. In response to ligand binding, IGF-1Rβ is translocated into the ER by β-arrestin2 (β-arr2). Mass spectrometry analysis identified SERCA2 as a target of ER IGF-1Rβ. SERCA2 activity is heavily dependent on the increase in ER IGF-1Rβ levels. ER IGF-1Rβ phosphorylates SERCA2 on Tyr^{990} to enhance its activity. Mutation of SERCA2-Tyr^{990} disrupted the interaction of ER IGF-1Rβ with SERCA2, and therefore ER IGF-1Rβ failed to promote SERCA2 activity. The enhancement of SERCA2 activity triggered Ca^{2+}_{ER} perturbation, leading to an increase in autophagy. Thapsigargin blocked the interaction between SERCA2 and ER IGF-1Rβ and therefore SERCA2 activity, resulting in inhibition of HCC growth. In conclusion, the translocation of IGF-1R into the ER triggers Ca^{2+}_{ER} perturbation by enhancing SERCA2 activity through phosphorylating Tyr^{990} in HCC.

*Corresponding authors. Tel./fax: +86 10 83911516.
E-mail addresses: cuisx@ccmu.edu.cn (Shuxiang Cui), qxj@ccmu.edu.cn (Xianjun Qu).

Peer review under the responsibility of Chinese Pharmaceutical Association and Institute of Materia Medica, Chinese Academy of Medical Sciences.

https://doi.org/10.1016/j.apsb.2023.05.031

1. Introduction

Insulin-like growth factor 1 (IGF1) receptor (IGF-1R), a tetrameric transmembrane receptor tyrosine kinase, is composed of two α and two β subunits linked by disulfide bonds. Upon ligand binding, β subunits are internalized to activate the insulin receptor substrate-initiated phosphatidylinositol 3-kinase (PI3K)−AKT−mammalian target of the rapamycin pathway, which predominantly leads to metabolic changes, and the SHC-initiated Ras−mitogen-activated protein kinase pathway, which promotes mitogenic changes[1]. IGF-1R is highly expressed in many cancer types[2,3]. Therefore, targeting IGF-1R is a promising strategy in cancer drug development. However, IGF-1R inhibitors frequently fail to be effective[4−6]. The IGF1/IGF-1R signaling pathway is more complex than anticipated due to its complex relationships with numerous other cellular signaling pathways, rendering tumor cells resistant to anti-IGF-1R therapy.

Sarco-endoplasmic reticulum calcium ATPase (SERCA) pumps are membrane transport proteins bound to the endo- or sarcoplasmic reticulum[7], playing essential roles in calcium transport from the cytoplasm into the endoplasmic reticulum (ER) to replenish the stored calcium, which is necessary for protein folding chaperones, calnexin, and calreticulin. However, overexpression of SERCA could trigger Ca^{2+}_{ER} perturbation, leading to the unfolded protein response[8]. Three SERCA isoforms, including SERCA1, SERCA2, and SERCA3, were identified as being highly expressed in the specialized ER, where they account for ∼50% of all membrane proteins[9]. The importance of SERCA pumps in cancer was recently highlighted by the finding that SERCA pumps are overexpressed in many cancer types[10]. These cancers involve the dysregulation of calcium signaling to mediate critical cellular processes, including the transcriptional regulation which underlies gene expression in a wide range of pathways crucial to tumorigenesis, such as proliferation, angiogenesis, migration, cell cycle progression, immune system evasion, and bypass of autophagy[11]. However, the SERCA isoforms that are specifically dysregulated in cancer subtypes have not been identified, and little is known about their pathological functions. SERCA1, the isoform that is expressed in fast-twitch skeletal muscle tissue, has not been identified in cancer cells[12]. SERCA2 (encoded by *ATP2A2*) has been found to be overexpressed in several cancer types, including colon cancer, hepatocellular carcinoma (HCC), lung cancer, breast cancer, neuroglioma, and prostate cancer[13]. The expression levels and pathological functions of SERCA3 in tumorigenesis are still controversial[14]. Cancer cells can hijack SERCAs, which are functional calcium pumps, to transform calcium transients such that they support a constitutively active and dividing state. Therefore, targeting SERCA results in the inhibition of prostate cancer and neuroglioma cells by blocking the transformation of calcium transients[15].

In the present study, we provide evidence that activation of the IGF-1R signaling pathway stimulates cancer growth through the translocation of IGF-1Rβ into the ER to activate SERCA2, leading to Ca^{2+}_{ER} perturbation in HCC cells. This in turn leads to activation of the PERK−eIF2α−ATF4 signaling pathway, resulting in ER stress and triggering autophagy in HCC cells. Immunoprecipitation assays followed by mass spectrometry showed that ER IGF-1Rβ interacts with SERCA2. We further found that ER IGF-1Rβ stimulates SERCA2 activity by phosphorylating the Tyr^{990} residue of SERCA2. Thapsigargin, a SERCA2 inhibitor, inhibited HCC growth by blocking the interaction of ER IGF-1Rβ with SERCA2.

2. Material and methods

2.1. Reagents

Bafilomycin A1 (Baf A1, HY-10058) and thapsigargin (HY-13433) were purchased from MCE (New Jersey, USA). LY294002 (S1105) and NVP-AEW541 (S1034) were purchased from Selleck (Houston, TX, USA). Fetal bovine serum (42F6590K) and Dulbecco's modified Eagle's medium (10373017) were obtained from Gibco (NY, USA). Human IGF1 (100-11-100UG) was purchased from PeproTech (New Jersey, USA). The Minute™ Plasma Membrane Protein Isolation and Cell Fractionation Kit (SM-005) and the Minute™ ER Enrichment Kit (ER-036) were provided by Invent Biotechnologies (Eden Prairie, Minnesota, USA).

2.2. Cell lines and cell culture

The HCC cell lines HepG2, PLC/PRF/5, and Hep3B and the normal human liver cell line HepRG were all obtained from the China Cell Collection (Shanghai, China). Cells were cultured in an incubator at 37 °C and 5% CO_2 in Dulbecco's modified Eagle's medium supplemented with 10% fetal bovine serum.

2.3. Plasmid constructs

GFP-IGF-$1R^{999\text{-end}}$, full-length wild-type SERCA2 with a C-terminal Flag-tag, Flag-$SERCA2^{294/295}$, and Flag-$SERCA2^{990}$ cDNA were amplified in HEK293T cells by standard PCR and cloned in pcDNA3.1(+) plasmids. Deletion and truncation of cDNA were amplified in HEK293T cells and subcloned into pcDNA3.1(+) GFP plasmids. Mutation cDNA was amplified in HEK293T cells and subcloned into pcDNA3.1(+) Flag plasmids. Plasmids were transiently transfected into HEK293T cells using Lipofectamine 3000 reagent (L3000015, Invitrogen, USA) according to the manufacturer's instructions.

2.4. RNA interference assay and lentiviral transfection assay

Small interfering RNA (siRNA) was designed by GenePharma (Suzhou, China). Human siIGF-1R, siATP2A2-1, and siATP2A2-2 were routinely co-transfected into cells using Lipofectamine 2000 (11668019, Invitrogen, USA) and an equal volume of siRNA suspension (siRNA sequences are detailed in Supporting Information Table S1). Short hairpin RNA (shRNA) was purchased

from GenePharma (Suzhou, China). Cells were plated in six-well plates and incubated for 24 h before RNA interference. Diluted polybrene was lightly mixed with an equal volume of shRNA suspension in DMEM (shRNA sequences are detailed in Supporting Information Table S2). Each sample was incubated at 37 °C for 12 h. The medium was replaced, and the cells were incubated for 48 h to confirm the infection rate.

2.5. HCC patient specimens and immunohistochemical analysis

The use of human samples was approved by the Ethics Committee of BinZhou Hospital (2018-81772637-01). All patients have provided written informed consent. A total of 46 randomly selected HCC specimens obtained from 2018 to 2019 were used to analyze the levels of IGF1, IGF-2, and IGF-1R in HCC tissues. Antibody information is shown in Supporting Information Table S3. Immunohistochemistry (IHC) scores were determined as follows: ≤10% of stained cells (−); 11%−25% of stained cells (+); 26%−50% of stained cells (2+); and ≥51% of stained cells (3+).

2.6. Immunofluorescence assay

The immunofluorescence assay was routinely performed as previously described[16].

2.7. Calcium labeling and confocal microscopy analysis

HCC cells were loaded with 20 μmol/L Fluo-4-AM (F14201, ThermoFisher Scientific, USA) or 20 μmol/L Mag-fluo-4-AM (M14206, ThermoFisher Scientific, USA) and imaged under a Zeiss LSM510 confocal microscope in a frame scan mode for ∼10 s. Then the cells were exposed to 50 nmol/L IGF1, and images were continuously taken for ∼600 s. The amplitude of the peak Ca^{2+} transient was calculated as Eq. (1):

$$\text{Amplitude} = (F - F_0)/F_0 \quad (1)$$

where F represents the maximum value of a Ca^{2+} transient and F_0 represents the Ca^{2+} level immediately before the onset of a Ca^{2+} transient[17].

2.8. Silver staining and mass spectrometry

Proteins were separated by 8% SDS-PAGE and visualized by silver staining. Gel bands were excised and then subjected to in-gel trypsin digestion. The peptides were separated and analyzed on a TRIPLETOF 6600 mass spectrometer. About 4 μL of peptides were injected into a C18AQ column (3 μm, 120 Å, 35 μm × 0.5 mm) at a flow rate of 600 nL/min. Mobile phase A (0.1% formic acid in 2% acetonitrile) and mobile phase B (0.1% formic acid in 98% acetonitrile) were used to establish a 90 min gradient of 0 min 5% B; 45 min of 5%−22% B; 10 min of 22%−30% B; 10 min of 30%−45% B; 10 min of 45%−90% B; and 15 min of 95% B. Mass spectrometry conditions were as follows: ESI ion source, positive ion mode, a spray voltage of 2.3 kV, and an ion temperature of 150 °C. All mass spectrometry analyses were performed by the proteomics platform of Capital Medical University.

2.9. Western blot and co-immunoprecipitation assays

Western blot and co-immunoprecipitation (Co-IP) assays were routinely performed as previously described[18,19]. Antibody information is provided in Supporting Information Table S3.

2.10. SERCA2 activity measurement

SERCA2 activity was assessed using a colorimetric ATPase assay kit (A070-4-2, Nanjing Jiancheng Bioengineering Institute, China). ATPase activity was normalized to protein content[20].

2.11. Human HCC cells xenografted in livers of nude mice and thapsigargin treatment

The experimental protocol was approved by the Animal Welfare Committee of Capital Medical University (AEEI-2020-094). BALB/c nude mice were provided by Charles River Laboratories (Beijing, China). HepG2 cells (1×10^6 cells in 0.15 mL normal saline [NS]) were injected into the medial lobe of the liver. Mice were randomly divided into the following groups: (i) normal mice receiving NS; (ii) mice with HepG2 xenograft receiving NS; (iii) mice with HepG2 xenograft receiving 1 mg/kg of rhIGF1[21]; (iv) mice with HepG2 xenograft receiving thapsigargin (10 mg/kg/day) *via* the caudal vein in three consecutive weeks[22]; and (v) mice with HepG2 xenograft receiving 1 mg/kg of rhIGF1+thapsigargin. Mice were euthanized; visible metastatic nodules were observed in mice livers, which were fixed for further analysis.

2.12. Statistical analysis

Data are described as mean ± standard deviation (SD). Statistical analysis was performed with SPSS/Win19.0 software (SPSS, Chicago, IL, USA). Comparisons between the IGF1-treated and control mice were conducted with a two-tailed Student's *t*-test. A P value of <0.05 was considered to be statistically significant. Spearman correlation was used to analyze the association between IGF1/IGF2 and IGF-1R in human HCC tissues.

3. Results

3.1. Activation of IGF1/IGF-1R signaling in human HCC tissues

The Cancer Genome Atlas RNA-seq data did not show higher levels of *Igf-1r*, *Igf1*, and *Igf2* in HCC tissues than in healthy people (Supporting Information Fig. S1A). However, we identified higher levels of IGF-1R, IGF1, and IGF2 in HCC tissues than in their paired paracancerous tissues. All 46 HCC specimens had IGF-1R, IGF1, and IGF2 staining intensity of ≥51% stained cells (score 3+) in the HCC tissues. Comparably, weak (+) or moderate (2+) staining of IGF-1R, IGF1, and IGF2 was seen in the paired paracancerous tissues (Fig. S1B).

3.2. In response to ligand binding, IGF-1Rβ was translocated into the ER in HCC cells

It is well known that in response to ligands binding, IGF-1R is internalized through binding with clathrin and β-arrestins, followed by proteasomal degradation to cease IGF-1R

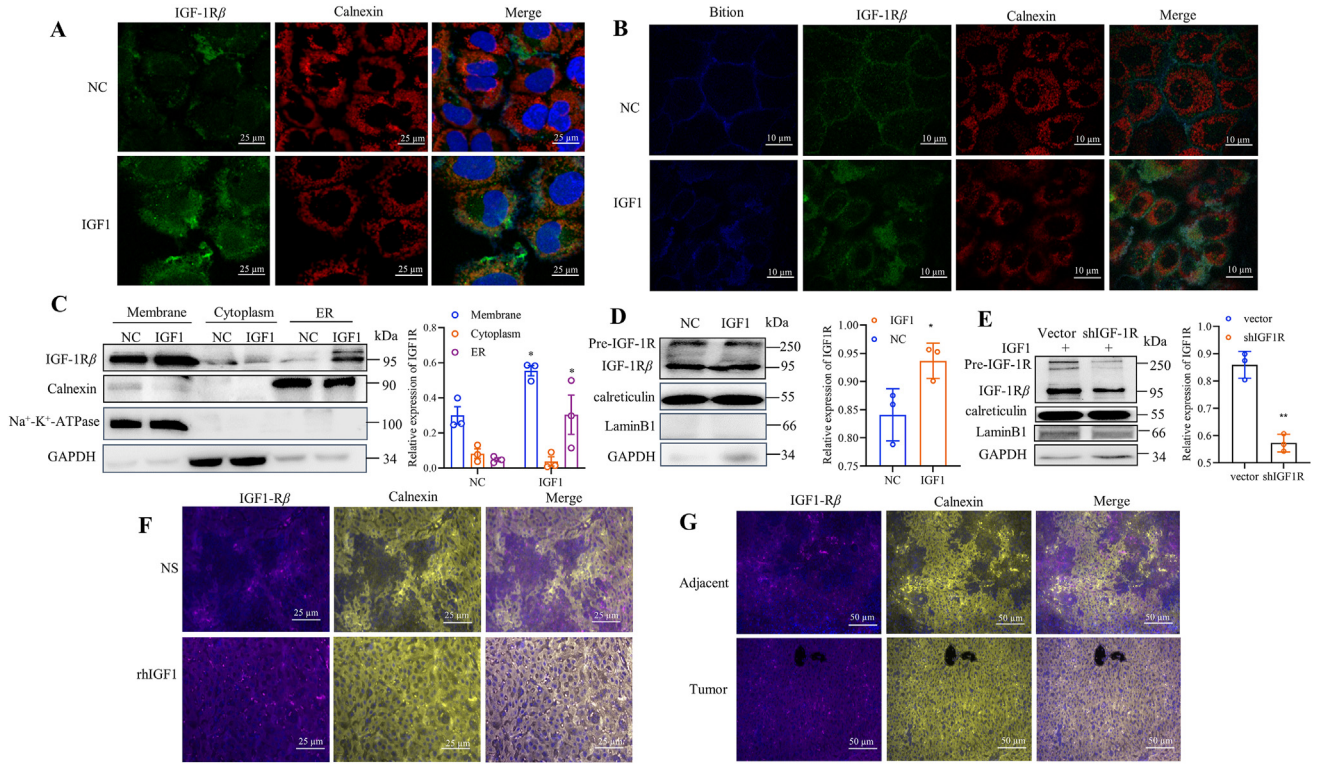

Figure 1 In response to ligand binding, IGF-1Rβ is translocated into the ER. (A) Immunofluorescence analysis of ER IGF-1Rβ in Hep3B cells exposed to 50 nmol/L IGF1 for 30 min. IGF-1Rβ (green), calnexin (red), nucleus (blue). Scale bar: 25 μm. (B) Immunofluorescence analysis showed the trajectory of biotinylated IGF-1R from the cell membrane to the ER. Scale bar: 10 μm. Intensity profiles indicate the protein levels along the plotted lines as determined by ImageJ. (C) Western blot assay of IGF-1Rβ extracted from the cell membrane, the cytoplasm, and the ER fraction in HepG2 cells. Data are presented as mean ± SD; $*P < 0.05$ ($n = 3$, Student's t test) compared to NC cells. (D) Western blot assay of IGF-1Rβ in the ER fraction of HepG2 cells. IGF-1Rβ = 95 kDa, pre-IGF-1R = 250 kDa. Data are presented as mean ± SD; $*P < 0.05$ ($n = 3$, Student's t test) compared with NC cells. (E) After silencing of IGF-1R, IGF1 failed to increase ER IGF-1Rβ levels in HepG2 cells. Data are presented as mean ± SD; $**P < 0.01$ ($n = 3$, Student's t test) compared to vector-transfected cells. (F) Immunofluorescence assay of ER IGF-1Rβ in HepG2 xenografts. IGF-1Rβ (purple), calnexin (yellow), nucleus (blue). The merged image shows the rhIGF1-treated liver and the NS-treated liver ($n = 6$). Scale bar: 25 μm. (G) Immunofluorescence assay of ER IGF-1Rβ, showing the IGF-1R/calnexin colocalization in HCC tissues but not obviously in the paired paracarcinoma tissues. $n = 6$, scale bar: 50 μm.

signaling[23,24]. However, we identified a disobliging IGF-1R signaling pathway in the ER. This disobliging IGF-1R signaling was not observed in normal human liver cells. Immunofluorescence assays showed that IGF-1Rβ was localized in the ER of HCC cells treated with 50 nmol/L IGF1[25] for 30 min (Fig. 1A for Hep3B cells and Supporting Information Fig. S2A for HepG2 cells). The trajectory of the biotinylated IGF-1Rβ indicated that IGF-1Rβ was translocated from the cell membrane to the ER (Fig. 1B). The translocation of IGF-1Rβ was further confirmed by analyzing its molecular mass (Fig. 1D and 95 kDa) in the subcellular fractions of HCC cells (Fig. 1C). Because the IGF-1R precursor is synthesized in the ER and then cleaved into α and β subunits in the Golgi apparatus[26], we also identified it in the ER (250 kDa, Fig. 1D and Fig. S2B). Knockdown of IGF-1R impeded the IGF1-driven translocation of ER IGF-1Rβ in HepG2 cells (Fig. 1E) and Hep3B cells (Fig. S2C). The presence of ER IGF-1Rβ was further confirmed in HepG2 xenografts. Immunofluorescence analysis showed that IGF-1Rβ was present in the ER in IGF1-treated mice but not in NS-treated mice (Fig. 1F). ER IGF-1Rβ was also identified in human HCC tissues but not in their paired paracancerous tissues (Fig. 1G).

3.3. β-Arr2 but not β-arr1 mediated the translocation of ER IGF-1Rβ in HCC cells; this translocation was not observed in normal human liver cells

As IGF-1Rβ was translocated into the ER, we explored the mechanism of this translocation. Expectedly, IGF-1Rβ was internalized through binding with clathrin in response to IGF1 for 20 min in HCC cells (Supporting Information Fig. S3A). Interestingly, co-expression of IGF-1Rβ and clathrin initiated a dynamic process; at 30 min after IGF1 exposure, the levels of clathrin were not further increased (Fig. S3B), while β-arr2 but not β-arr1 levels gradually increased (Fig. 2A). β-Arr2 was also identified in the ER (Supporting Information Fig. S4B–S4D). Immunofluorescence assays showed the β-arr2-mediated translocation of IGF-1Rβ into the ER at 30 min, and co-expression of β-arr2 with IGF-1Rβ was blunted at 40 min (Fig. S4A). The Co-IP assay revealed the co-expression of IGF-1Rβ with β-arr2 (Fig. 2B—i) but not the co-expression of IGF-1Rβ with β-arr1 in HepG2 cells (Fig. 2B—ii). The β-arr2 inhibitor Barbadin and silencing of β-arr2 both blocked the IGF1-driven co-expression of IGF-1Rβ and β-arr2 in the ER of HCC cells (Fig. 2C and D).

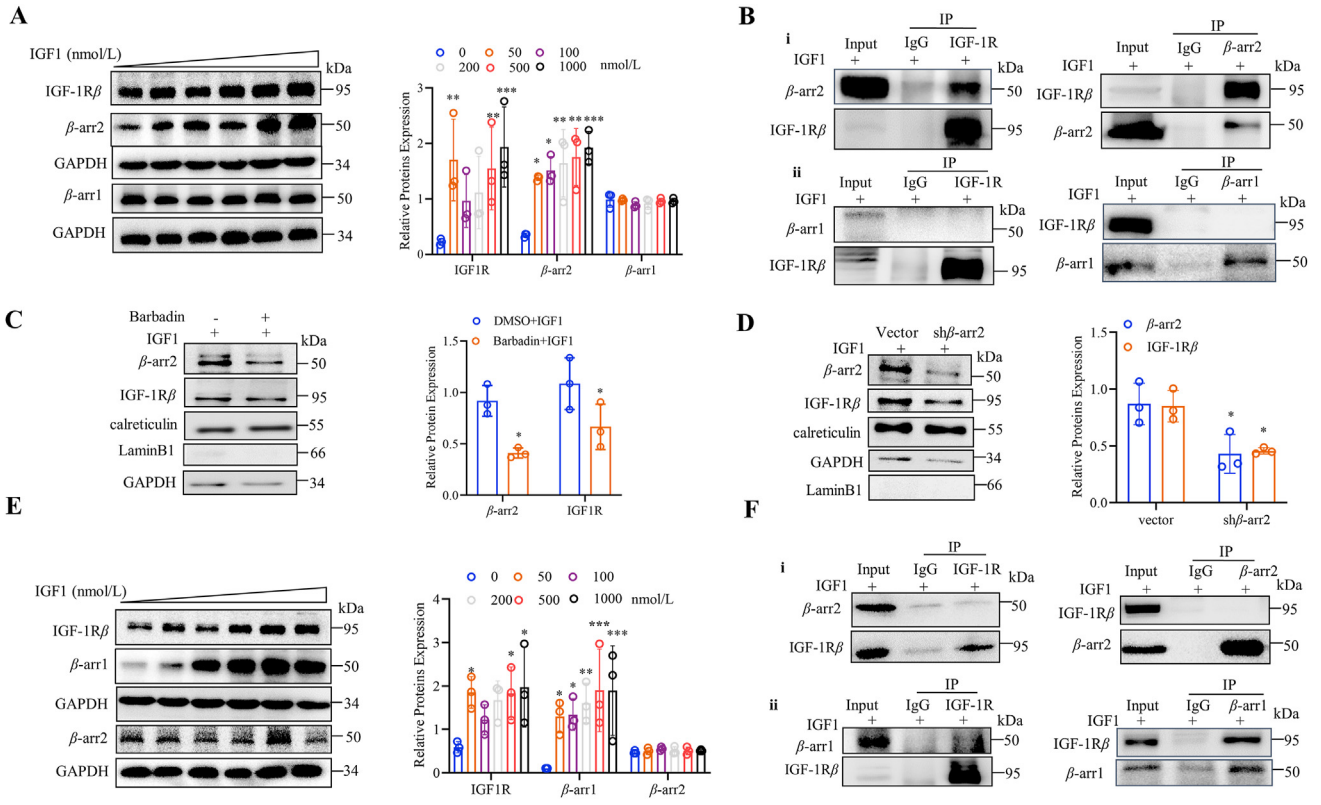

Figure 2 β-Arr2 but not β-arr1 mediates the translocation of ER IGF-1Rβ in HCC cells. (A) β-Arr2 but not β-arr1 was gradually increased in HepG2 cells exposed to increasing IGF1 levels (0−1000 nmol/L). Data are presented as mean ± SD; $*P < 0.05$, $**P < 0.01$, $***P < 0.001$ ($n = 3$, Student's t test) compared with the cells without IGF1. (B) Co-IP assay showing that it is β-arr2 but not β-arr1 that interacts with IGF-1Rβ in the presence of IGF1 in HepG2 cells. (C) Western blot assay of the ER fraction showed that Barbadin (100 nmol/L, 30 min) blocked the IGF1-driven increase of IGF-1Rβ and β-arr2 in the ER of HepG2 cells. Data are presented as mean ± SD; $*P < 0.05$ ($n = 3$, Student's t test) compared with IGF1-treated cells. (D) After silencing of β-arr2, IGF1 failed to increase ER IGF-1Rβ and β-arr2 levels in the ER of HepG2 cells. Data are presented as mean ± SD; $*P < 0.05$ ($n = 3$, Student's t test) compared with the cells transfected with vector. (E) β-Arr1 but not β-arr2 was gradually increased in normal HepRG liver cells in the presence of increasing IGF1 levels (0−1000 nmol/L). Data are presented as mean ± SD; $*P < 0.05$, $**P < 0.01$, $***P < 0.001$ ($n = 3$, Student's t test) compared with the cells without IGF1. (F) Co-IP assay showing that β-arr1 but not β-arr2 interacts with IGF-1Rβ in the presence of IGF1 in normal HepRG liver cells.

Normal liver cells exhibited an increase of β-arr1 but not β-arr2 in the cytoplasm (Fig. 2E) and co-expression of IGF-1Rβ with β-arr1 but not co-expression of IGF-1Rβ with β-arr2 (Fig. 2F).

3.4. *SERCA2 was identified as a target of ER IGF-1Rβ*

As IGF-1Rβ was translocated into the ER, we next searched for ER IGF-1R's target. We first performed an SDS-PAGE assay to analyze the ER IGF-1Rβ interactome. As shown in Fig. 3A, the molecular weights of these proteins are mainly enriched above 80 kDa. These proteins were further subjected to mass spectrometry analysis to identify the proteins bound with ER IGF-1Rβ (Supporting Information Table S4). These ER IGF-1Rβ-binding proteins were mainly involved in metabolism and the calcium signaling pathway (Supporting Information Table S5). After data filtering and in-depth bioinformatics analysis, SERCA2 was finally identified as a target of ER IGF-1Rβ. SERCA2 was activated in response to IGF1 (Fig. 3B and C and Supporting Information Fig. S5A). After IGF-1R knockdown, ER IGF-1Rβ failed to activate SERCA2 in HepG2 cells (Fig. 3D and Fig. S5B and S5C). A Co-IP assay confirmed the co-expression of ER IGF-1Rβ with SERCA2 in HepG2 cells (Fig. 3E). The co-expression of ER IGF-1Rβ with SERCA2 was further identified in HepG2 xenografts exposed to IGF1 but not HepG2 xenografts exposed to NS (Fig. 3F). Also, the co-expression of ER IGF-1Rβ with SERCA2 was confirmed in HCC tissues but not in the paired paracancerous tissues (Fig. 3G).

3.5. *The increase of SERCA2 was dependent on the increase of phosphorylated ER IGF-1Rβ*

As ER IGF-1Rβ interacted with SERCA2, we analyzed the effect of this interaction. The $Tyr^{1131/1135/1136}$ residues in the kinase domain of IGF-1R were reported to be the earliest major sites of autophosphorylation necessary for kinase activation[27]. In this study, the increase of SERCA2 was dependent on IGF-1Rβ phosphorylation on Tyr^{1131} and $Tyr^{1135/1136}$ (Fig. 4A). Supportive of this conclusion, NVP-AEW541, an inhibitor of IGF-1R, blocked the IGF1-driven autophosphorylation of IGF-1Rβ on Tyr^{1131} and $Tyr^{1135/1136}$, and therefore IGF-1Rβ-induced SERCA2 activation was blocked in HepG2 cells (Fig. 4A). Analysis of the ER proteins confirmed the above conclusion (Fig. 4B). A Co-IP assay identified the interaction of IGF-1Rβ with SERCA2 in the ER, and this interaction was blocked by NVP-AEW541 (Fig. 4C).

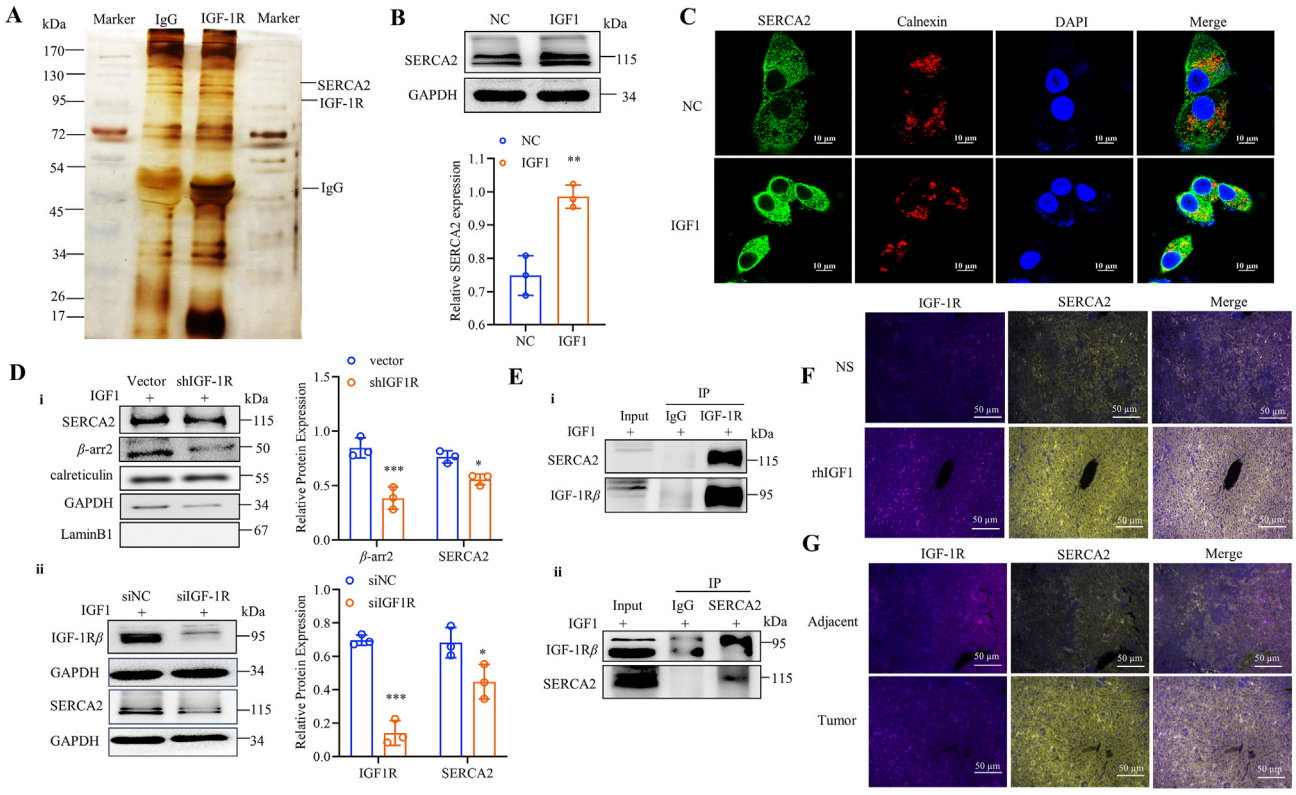

Figure 3 SERCA2 was identified as a target of ER IGF-1Rβ. (A) Immunoprecipitation assay followed by silver staining of the ER protein fraction isolated from HepG2 cells exposed to IGF1. Molecular weights of the proteins bound to IGF-1R were mainly >80 kDa. (B) SERCA2 responded to IGF1 stimulation in HepG2 cells. Data are presented as mean ± SD; $^{**}P < 0.01$ ($n = 3$, Student's t test) compared with NC cells. (C) Immunofluorescence staining analysis showed the co-localization of calnexin with SERCA2 responded to IGF1 for 30 min in Hep3B cells. Scale bar: 10 μm. (D-i) After knockdown of IGF-1R, the increase of β-arr2 and the ER IGF-1Rβ-induced activation of SERCA2 in HepG2 cells were impeded. Data are presented as mean ± SD; $^{*}P < 0.05$, $^{***}P < 0.001$ ($n = 3$, Student's t test) compared with the cells transfected with vector. (D-ii) After knockdown of IGF-1R, ER IGF-1Rβ failed to induce SERCA2 activity in HepG2 cells. Data are presented as mean ± SD; $^{*}P < 0.05$, $^{***}P < 0.001$ ($n = 3$, Student's t test) compared with the cells transfected with siNC. (E) Co-IP assay identified the IGF-1Rβ−SERCA2 complex in HepG2 cells exposed to IGF1. (F) Immunohistochemical fluorescence identified the IGF-1Rβ−SERCA2 complex in HepG2 xenografts treated with IGF1 *vs*. HepG2 xenografts without IGF1. $n = 6$. Scale bar: 50 μm. (G) Immunohistochemical fluorescence showed the IGF-1Rβ−SERCA2 complex in HCC tissues but not in the paired paracancerous tissues. $n = 6$. Scale bar: 50 μm.

To identify the functional motif of IGF-1Rβ necessary for SERCA2 binding, we constructed truncated IGF-1Rβ fragments including the tyrosine kinase region. A Co-IP assay identified $IGF\text{-}1R^{999\text{-end}}$ as the core region of the tyrosine kinase necessary for SERCA2 phosphorylation (Fig. 4D). Silencing of SERCA2 blocked the interaction of IGF-1Rβ with SERCA2 (Fig. 4E). Thapsigargin, a SERCA2 inhibitor, also decreased the interaction of ER IGF-1Rβ with SERCA2 in Hep3B cells (Fig. 4F).

3.6. Tyr^{990} phosphorylation of SERCA2 by ER IGF-1Rβ increased its activity

We examined the effect of the interaction between ER IGF-1Rβ and SERCA2. Theoretically, as a tyrosine kinase, ER IGF-1Rβ can phosphorylate its target SERCA2. Mass spectrometry analysis identified 16 distinct peptides of SERCA2 when ER IGF-1R was co-expressed with SERCA2 in IGF1-treated HepG2 cells (Supporting Information Table S6). An immunoprecipitation assay of the ER protein fraction followed by mass spectrometry identified the peptides containing the phosphorylated Tyr sites including NYLEPGK and GAIYYFK (Fig. 5A). Through this strategy, three possible Tyr sites (Tyr^{990}, Tyr^{294}, and Tyr^{295}) phosphorylated by ER IGF-1Rβ were identified. We mutated these three possible phosphorylated Tyr sites to the non-phosphorylatable alanine and then assayed their binding status. Mutation of Tyr^{990} but not Tyr^{294} and Tyr^{295} blocked the IGF1-stimulated interaction between ER IGF-1Rβ and SERCA2, indicating the key Tyr site of SERCA2 (Fig. 5B−i). These experimental results were consistent with the predicted results by the group-based phosphorylation site predicting and scoring platform. Group-based phosphorylation site prediction and the scoring platform predicted a higher phosphorylation score for Tyr^{990} than for Tyr^{294} and Tyr^{295} of SERCA2 (Fig. 5B−ii). Therefore, Tyr^{990} was identified as a key residue of SERCA2 that binds with phosphorylated ER IGF-1Rβ. A Co-IP assay indicated that this interaction was blunted by the Tyr^{990} mutation (Fig. 5C). Thus, in HCC cells with the Tyr^{990} mutation, IGF1 failed to increase SERCA2 activity (Fig. 5D).

3.7. Activation of SERCA2 enhanced the calcium transport activity, leading to Ca^{2+}_{ER} perturbation to activate PERK−eIF2α−ATF4 signaling

As a sarcoplasmic/ER calcium ATPase, SERCA2 regulates calcium transport from the cytosol into the ER for maintaining Ca^{2+}

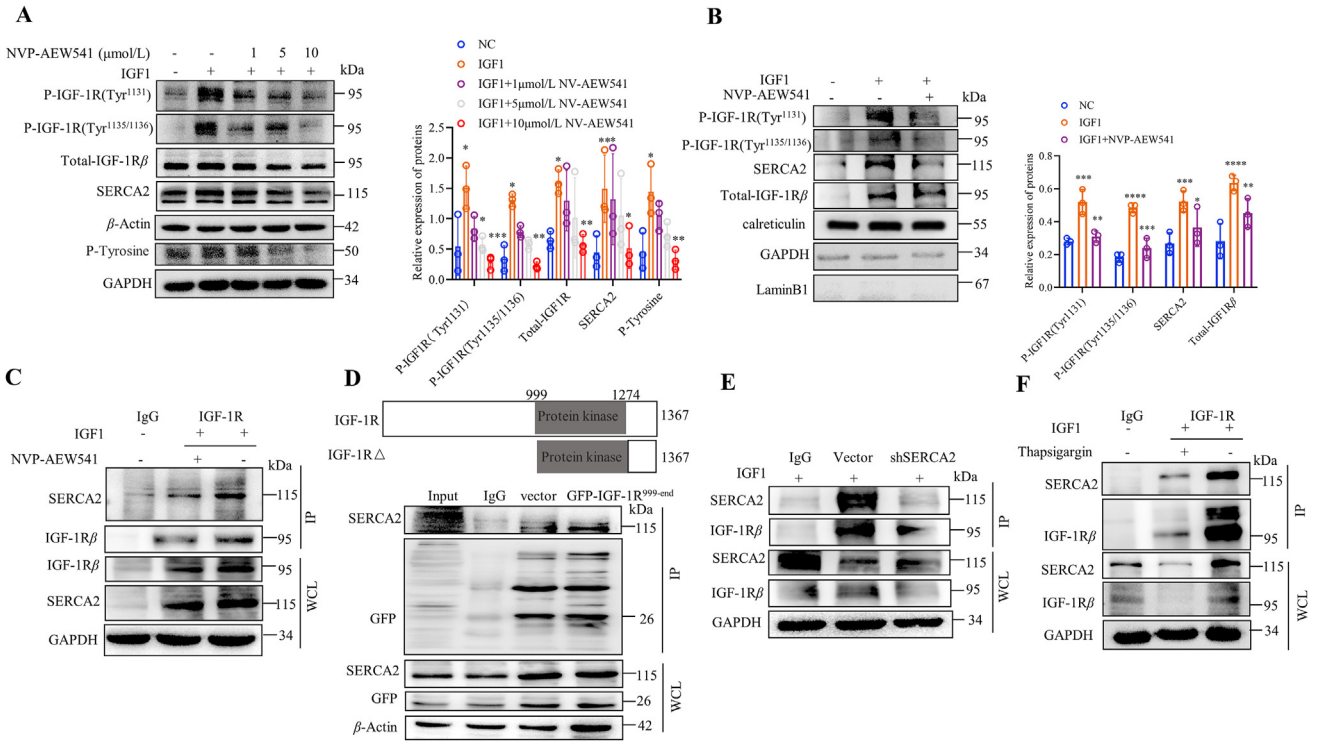

Figure 4 The increase in SERCA2 activity was dependent on the increase in phosphorylated ER IGF-1Rβ. (A) NVP-AEW541 blocked the IGF1-driven autophosphorylation of IGF-1Rβ on Tyr^{1131} and $Tyr^{1135/1136}$, and consequently decreased SERCA2 activity in HepG2 cells. Data are presented as mean ± SD; $*P < 0.05$, $**P < 0.01$, $***P < 0.001$ ($n = 3$, Student's *t*-test) compared with IGF1-treated cells without NVP-AEW541. (B) Western blot assay of the ER protein fraction showed that the IGF1-driven autophosphorylation of IGF-1Rβ on Tyr^{1131} and $Tyr^{1135/1136}$ was blocked by NVP-AEW541 (10 μmol/L, 12 h), and the level of SERCA2 was consequently reduced in the ER. Data are presented as mean ± SD; $*P < 0.05$, $**P < 0.01$, $***P < 0.001$ ($n = 3$, Student's *t* test) compared with the IGF1-treated cells without NVP-AEW541. (C) Co-IP assay shows that the IGF1-driven formation of the ER IGF-1Rβ−SERCA2 complex was significantly blunted by NVP-AEW54 (10 μmol/L, 12 h). (D) Co-IP assay to determine the interaction between SERCA2 and truncated-$IGF\text{-}1R^{999\text{-}1367}$ in HEK293T cells. The cells transfected with $IGF\text{-}1R^{999\text{-}end}$ retained the interaction of SERCA2 with ER IGF-1Rβ. (E) Silencing of SERCA2 blocked the interaction of ER IGF-1Rβ with SERCA2 in HepG2 cells in the presence of IGF1. (F) Thapsigargin (5 μmol/L, 24 h) decreased the interaction of ER IGF-1Rβ with SERCA2 in HepG2 cells in the presence of IGF1.

homeostasis[28,29]. As SERCA2 was activated (Fig. 6A), we analyzed the effect of this response in HCC cells. Mag-fluo-4, an ER calcium indicator[30], was used to analyze free Ca^{2+} levels in the ER, and fluo-4 was used to measure $Ca^{2+}_{cytoplasm}$ concentrations[31]. Compared to control cells, the cells exposed to IGF1 demonstrated a sharp decrease in $Ca^{2+}_{cytoplasm}$ within 10 s, and correspondingly, the Ca^{2+}_{ER} levels were drastically increased at the same time, which maintained higher levels within 600 s. Control cells maintained relatively stable Ca^{2+}_{ER} and $Ca^{2+}_{cytoplasm}$ levels during this time (Fig. 6B and C). These results indicate that the increased Ca^{2+}_{ER} was due to the sharply reduced $Ca^{2+}_{cytoplasm}$. The PI3K−Akt inhibitor LY294002 did not block the IGF1-induced Ca^{2+}_{ER} perturbation (Fig. 6D). In the same condition of IGF1 exposure, normal human liver cells did not exhibit the Ca^{2+}_{ER} perturbation (Fig. 6E).

As a sensor of ER stress, glucose-regulating protein 78 (GRP78) functions as a molecular chaperone in the ER that regulates ER stress signaling in response to Ca^{2+}_{ER} perturbation[32]. Thus, ER IGF-1Rβ-induced Ca^{2+}_{ER} perturbation led to ER stress by activating the GRP78−PERK−eIF2α−ATF4 pathway (Fig. 6F). Silencing of IGF-1R impeded the translocation of ER IGF-1Rβ and thus blocked the GRP78−PERK−eIF2α−ATF4 pathway (Fig. 6G). Further, silencing of SERCA2 impeded the binding of ER IGF-1Rβ with its target and thus blocked the GRP78−PERK−eIF2α−ATF4 pathway (Fig. 6H).

3.8. Activation of the PERK−eIF2α−ATF4 signaling induced by Ca^{2+}_{ER} perturbation triggered autophagy in HCC cells; thapsigargin blocked the binding of ER IGF-1Rβ with SERCA2, resulting in the inhibition of HCC

Expectedly, HCC cells exhibited autophagy initiation in response to the activated GRP78−PERK−eIF2α−ATF4 pathway (Fig. 7A-i−iii). These HCC cells exhibited turnover of LC3, showing an increase of LC3-I, and correspondingly the LC3-II level was increased in the presence of Baf A1 (Fig. 7A-ii−iii). As a result, the autophagy-related proteins Beclin1, LC3B-I/II, and SQSMT1/p62 were significantly increased in the above autophagic HCC cells (Supporting Information Fig. S6A). Silencing of IGF-1R and SERCA2 blocked IGF1-induced autophagy in HepG2 and Hep3B cells (Fig. S6B and S6C).

The effects of ER IGF-1Rβ-stimulated SERCA2 were confirmed in HepG2 xenografts. Nude mice were treated with NS, rhIGF1 (1 mg/kg/day *via* the caudal vein), and rhIGF1+thapsigargin (10 mg/kg/day *via* the caudal vein). HepG2 xenografts grew quickly, showing moderately spread HCC nodules in the

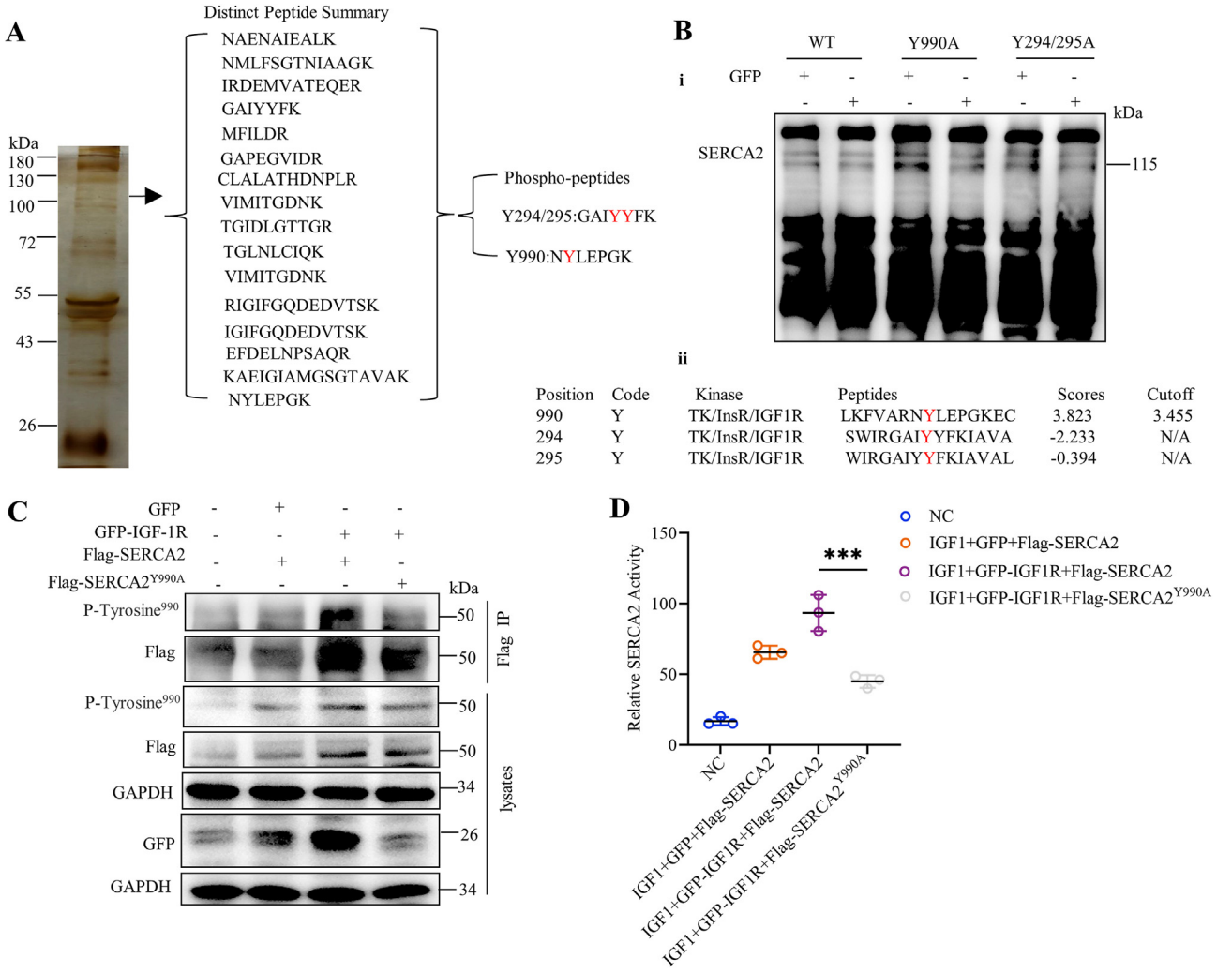

Figure 5 ER IGF-1Rβ interacted with SERCA2, leading to enhanced SERCA2 activity through Tyr^{990} phosphorylation. (A) Mass spectrometry analysis of the proteins co-immunoprecipitated with ER IGF-1Rβ in IGF1-treated HepG2 cells. Three phosphorylation sites including Tyr^{990}, Tyr^{294}, and Tyr^{295} of SERCA2 were identified (marked in red). (B-i) Mutation of three possible Tyr phosphorylation sites of SERCA2 showed that Tyr^{990} but not Tyr^{294} and Tyr^{295} was the core residue of SERCA2 in HepG2 cells. (B-ii) The group-based phosphorylation site prediction and scoring platform predicted that the phosphorylation score of Tyr^{990} was higher than those of Tyr^{294} and Tyr^{295} of SERCA2. (C) Co-IP analysis showing that the binding of SERCA2 with ER IGF-1Rβ was blunted by Tyr^{990} mutation in IGF1-treated HEK293T cells. (D) The IGF1-driven increase of SERCA2 activity was blocked in the cells with Tyr^{990} mutation. Data are presented as mean ± SD; $^{***}P < 0.001$ ($n = 3$, Student's t-test) compared with the IGF1+GFP-IGF-1R + Flag-SERCA2-treated cells.

liver (Fig. 7B-ii–ii'). IGF1 stimulated HCC growth, showing more and larger metastatic nodules than in the mice treated with NS (Fig. 7B-iii–iii'). Thapsigargin moderately inhibited the formation of HCC nodules in mice without IGF1 (Fig. 7B-iv–iv'), while it strongly reduced the formation of HCC nodules in the presence of IGF1 (Fig. 7B-v–v'). An IHCassay showed increased SERCA2, GRP78, LC3B, and SQSMT1/p62 levels in the rhIGF1-treated HepG2 xenografts (Supporting Information Fig. S7, third column). Thapsigargin inhibited the rhIGF1-stimulated SERCA2 activity and the increase of these autophagy-related proteins (Fig. S7, fifth column).

4. Discussion

It is well known that the IGF1/IGF-1R signaling pathway activates variable processes, such as cell growth, cell differentiation, and survival, through activating the Ras–MAPK pathway and the PI3K pathway[1]. IGF-1R is highly activated in many cancer types[2,3]. However, higher levels of IGF1/IGF-1R signaling were specifically identified in liver cells, probably due to the IGFs predominantly produced by this organ[33]. Further, the loss of function of certain tumor suppressors can also increase IGF-1R expression, especially in liver cells. For example, the tumor suppressor p53 can suppress the transcription of *IGF-1R*, thereby decreasing the expression of *IGF-1R*. Mutations in tumor suppressors including p53 occur more frequently in the liver than in other organs[34]. Thus, dysregulation of IGF/IGF-1R signaling frequently occurs, controlling HCC stemness in the liver, which leads to tyrosine kinase inhibitor resistance and tumor recurrence[33]. In this study, we found that ER IGF-1R was translocated from the membrane of HCC cells by β-arr2. ER IGF-1Rβ phosphorylated SERCA2 on Tyr^{990}, leading to increased SERCA2 activity, resulting in Ca^{2+}_{ER} perturbation in HCC cells.

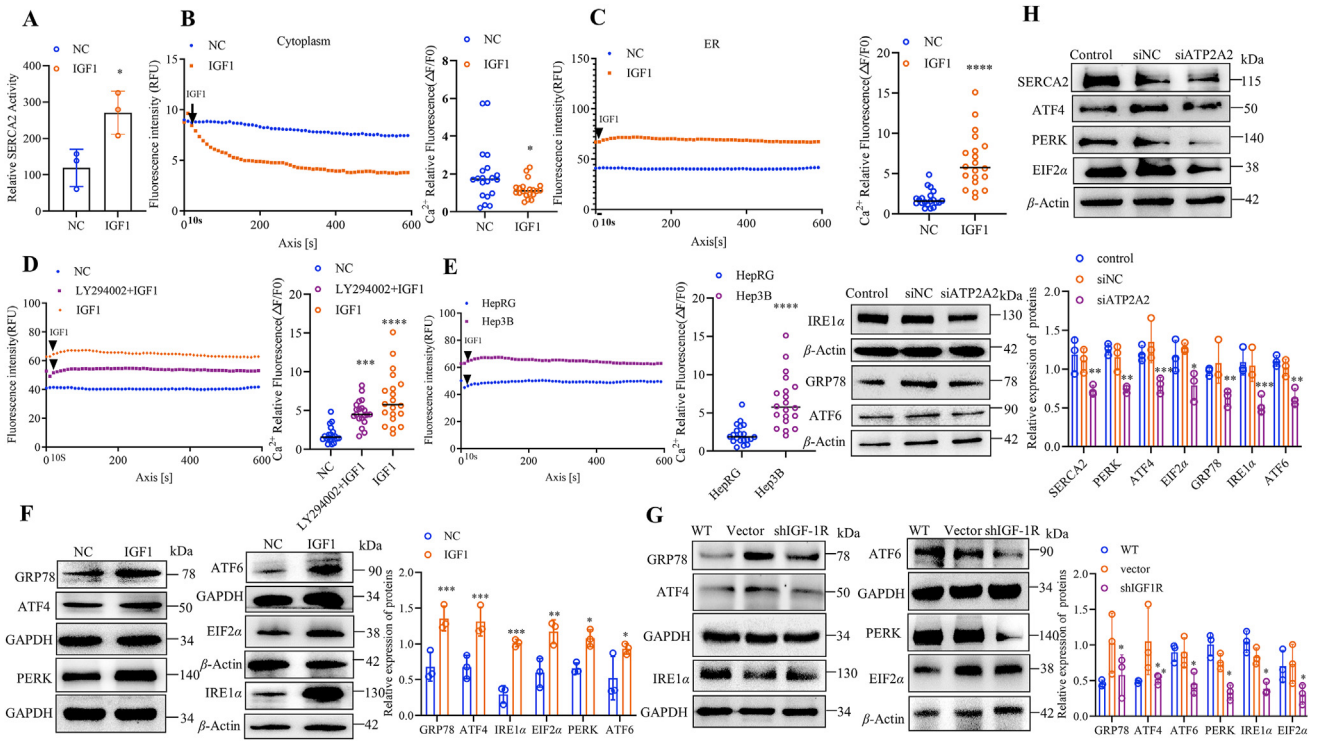

Figure 6 Activation of SERCA2 triggered Ca^{2+}_{ER} perturbation, leading to the activation of PERK−eIF2α−ATF4 signaling in HCC cells. (A) The levels of SERCA2 were increased in the presence of IGF1 in HepG2 cells. Data are presented as mean ± SD; *$P < 0.05$ compared with NC cells. (B, C) As compared to control cells, Hep3B cells exposed to IGF1 showed a sharp decrease of $Ca^{2+}_{cytoplasm}$ within 10 s, and correspondingly, the Ca^{2+}_{ER} levels were drastically increased in the same time, which maintained the higher levels within 600 s. *$P < 0.05$ compared with NC cells in the ER; ****$P < 0.0001$ compared with NC cells in the cytoplasm. (D) In Hep3B cells pretreated with LY294002 (1 nmol/L) for 30 min and treated with IGF1, the SERCA2-triggered Ca^{2+}_{ER} perturbation was not blocked. ****$P < 0.0001$ compared with NC cells. (E) Comparison of Ca^{2+}_{ER} levels between normal human liver cells and HCC cells in the presence of IGF1. Normal human liver cells had a lower Ca^{2+}_{ER} level than HCC cells under the same condition of IGF1 exposure. ****$P < 0.0001$ compared with HepRG cells. (F) The IGF1-driven ER IGF-1Rβ induced the Ca^{2+}_{ER} perturbation, leading to activation of the GRP78−PERK−eIF2α−ATF4 pathway. Data are presented as mean ± SD; $n = 3$. *$P < 0.05$, **$P < 0.01$, ***$P < 0.001$ compared with NC cells. (G) Silencing of IGF-1R impeded the translocation of ER IGF-1Rβ and thus blocked the GRP78−PERK−eIF2α−ATF4 pathway. Data are presented as mean ± SD; $n = 3$. *$P < 0.05$ compared with the cells transfected with empty vector. (H) Silencing of SERCA2 impeded the translocation of ER IGF-1Rβ and thus blocked the GRP78−PERK−eIF2α−ATF4 pathway. Data are presented as mean ± SD; $n = 3$. *$P < 0.05$, **$P < 0.01$, ***$P < 0.001$ compared with NC cells.

As an RTK, IGF-1R can be internalized in response to ligand binding through interaction with clathrin- or caveolin-mediated vesicles, followed by proteasomal degradation to cease IGF-1R signaling[35]. The current studies on IGF-1R signaling are mainly concentrated on the following two modes. In one, IGF-1R is internalized by a tyrosine-based motif, and the ligand-driven IGF-1Rβ is targeted to the clathrin-coated membrane invagination[23]. In the other, a ubiquitin-based motif "borrows" the components of the G-protein-coupled receptor signal, such as β-arrestins, resulting in IGF-1R signal cessation[36]. However, these "borrowed" concepts of the G-protein-coupled receptor signal did not fully explain recent observations of the IGF-1R signaling pathway[24]. It is known that although β-arr1 and β-arr2 share a high degree of sequence and structural homology, they are not functionally redundant[37]. They can act as signaling molecules in their own right with unique cellular, physiological, and pathophysiological consequences[38]. Thus, different β-arrestin isoforms determine differential fates of the IGF-1R signal through their specificity in recognizing their substrates. In the present study, we identified a disobliging IGF-1R signaling that was translocated into the ER to stimulate SERCA2 activity. We identified that it is β-arr2 but not β-arr1 that mediates the translocation of ER IGF-1Rβ. This translocation of ER IGF-1R does not occur in human normal liver cells. Thus, the translocation of ER IGF-1Rβ is a unique pathophysiological process in cancer cells.

In light of the above, the following question is raised: does ER IGF-1Rβ affect cancer growth, and if so, how? SERCA2 was identified as a target of ER IGF-1Rβ by analyzing the proteins interacting with ER IGF-1Rβ. It is known that ER is the principal calcium storage organelle in cells, and one of the most critical determinants of calcium levels in the ER of most cell types is the activity of SERCA2[39]. SERCA2 functions as a calcium pump from the cytosol into the ER to replenish stored calcium[40]. Alterations in Ca^{2+} homeostasis lead to cell proliferation and differentiation, apoptosis, and disruption of calcium homeostasis, which have been suggested to contribute to cancer development[41]. In the present study, HCC cells with ER IGF-1Rβ showed a drastic increase in Ca^{2+}_{ER} due to the sharply reduced $Ca^{2+}_{cytoplasm}$, indicating Ca^{2+}_{ER} perturbation in HCC cells. GRP78, acting as a central stress sensor in the ER, can regulate ER stress signaling

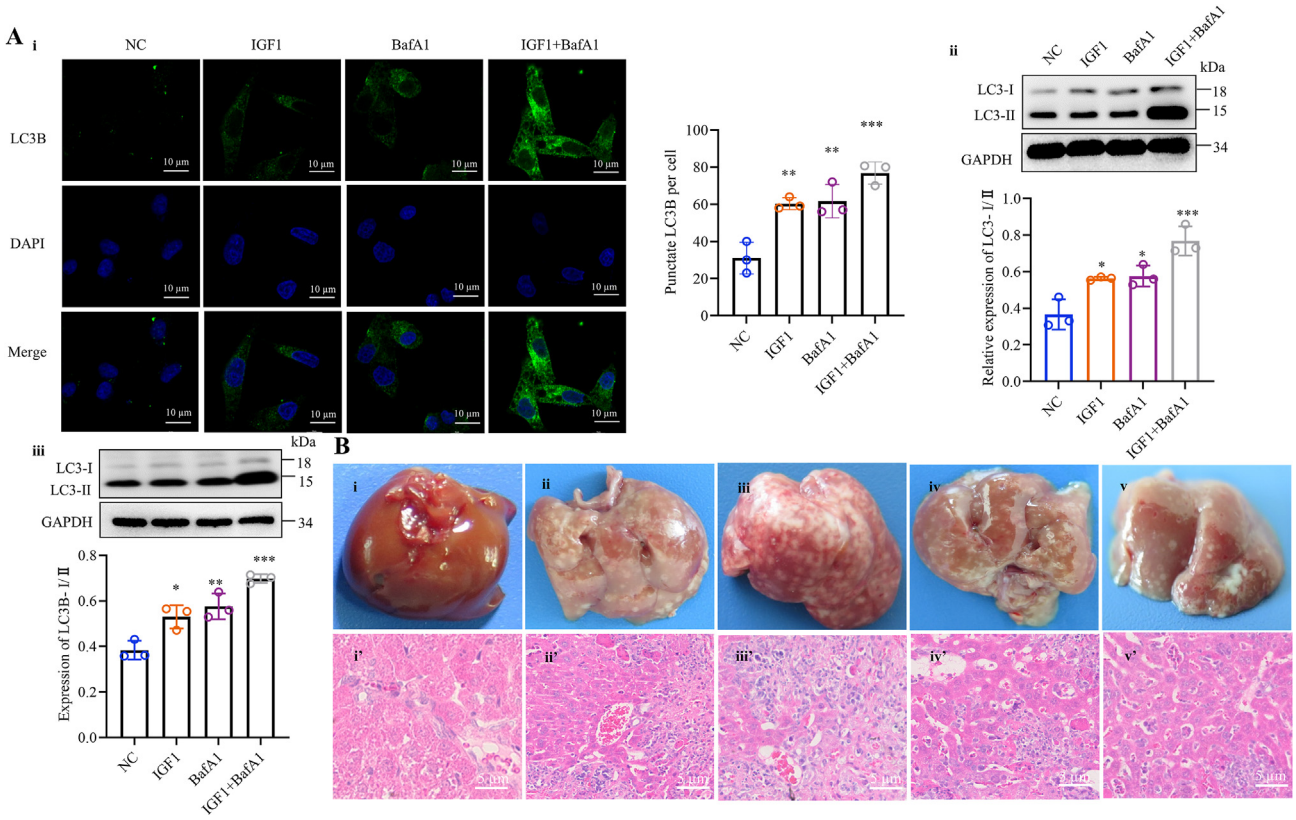

Figure 7 Activation of the PERK−eIF2α−ATF4 pathway triggered autophagy in HCC cells. Thapsigargin blocked the IGF1-driven binding of ER IGF-1Rβ with SERCA2, resulting in the inhibition of HCC. (A-i) Immunofluorescence analysis showed the autophagy indicated by LC3B in IGF1-treated HepG2 cells. Baf A1 (5 μmol/L for 12 h) increased the IGF1-induced autophagy. Data are presented as mean ± SD; $n = 3$. $^{**}P < 0.01$, $^{***}P < 0.001$ compared with NC cells. Scale bar: 10 μm. HCC cells with activation of the GRP78−PERK−eIF2α−ATF4 pathway exhibited turnover of LC3, showing increased LC3-I levels, and correspondingly the LC3-II level was further increased in the presence of Baf A1 in Hep3B cells (A-ii) and HepG2 cells (A-iii). Data are presented as mean ± SD; $n = 3$. $^{*}P < 0.05$, $^{**}P < 0.01$, $^{***}P < 0.001$ compared with NC cells. (B) Thapsigargin blocked the binding of ER IGF-1Rβ with SERCA2, resulting in the inhibition of HCC. (i, i') Mice treated with NS. (ii−ii') Mice with HepG2 xenografts treated with NS. (iii, iii') Mice with HepG2 xenografts treated with rhIGF1 (1 mg/kg/day *via* the caudal vein). (iv, iv') Mice with HepG2 xenografts treated with thapsigargin (10 mg/kg/day *via* the caudal vein). (v, v') Mice with HepG2 xenografts treated with rhIGF1+thapsigargin. First line: liver morphology, second line: HE images of livers. Scale bar: 5 μm.

once it senses alterations in Ca^{2+}_{ER}, leading to the unfolded protein response[42]. Thus, these HCC cells activate the PERK−eIF2α−ATF4 pathway in response to Ca^{2+}_{ER} perturbation.

Furthermore, another question is raised: how does ER IGF-1Rβ interact with SERCA2? It has been reported that $Tyr^{1131/1135/1136}$ in the kinase domain of IGF-1R are the earliest major sites of autophosphorylation necessary for kinase activation[43]. We thus analyzed the phosphorylated status of IGF-1Rβ on these sites in the ER. NVP-AEW541, an inhibitor of IGF-1R kinase on Tyr^{1131} and $Tyr^{1135/1136}$[44], blocked the IGF1-driven autophosphorylation on Tyr^{1131} and $Tyr^{1135/1136}$ in the ER. The phosphorylated ER IGF-1R interacted with SERCA2, leading to increased SERCA2 activity. To confirm this conclusion, we constructed truncated IGF-1Rβ fragments containing the tyrosine kinase region. A Co-IP assay identified $IGF\text{-}1R^{999\text{-}end}$ as the core region in the binding of ER IGF-1Rβ with SERCA2.

To explore the residues of SERCA2 which were phosphorylated by ER IGF-1R, we analyzed the interacting proteins when SERCA2 was co-expressed with ER IGF-1Rβ. As such, we considered whether this phosphorylation regulates SERCA2 activity. We performed mass spectrometry to analyze the interactome of SERCA2 co-expressed with ER IGF-1Rβ in the IGF1-treated HCC cells. Three possible phosphorylated Tyr sites including Tyr^{990}, Tyr^{294}, and Tyr^{295} of SERCA2 were identified. We mutated these possible phosphorylated Tyr sites to alanine and then assayed their binding status. Through this strategy, Tyr^{990} was identified as a key residue of SERCA2 bound with ER IGF-1Rβ. This binding was blunted by mutation of Tyr^{990}. Thus, ER IGF-1Rβ-stimulated SERCA2 activity was inhibited in these HCC cells. Tyr^{990} was identified as a key residue of SERCA2. The interaction of ER IGF-1Rβ with SERCA2 resulted in the enhancement of SERCA2 activity through Tyr^{990} phosphorylation in HCC cells.

Significantly, thapsigargin inhibited SERCA2 pumps[45], thus blocking the IGF1-stimulated binding of ER IGF-1Rβ with SERCA2, resulting in the inhibition of IGF1-stimulated HCC growth. The nude mouse model with HCC xenograft confirmed the inhibitory effect of thapsigargin on IGF1-stimulated HCC, indicating activation of IGF-1R signaling is a promising therapeutic strategy for various cancer types.

5. Conclusions

In this study, we found that in response to ligand binding, IGF-1R was translocated into the ER to enhance SERCA2 activity through phosphorylating SERCA2 on Tyr^{990}. This resulted in Ca^{2+}_{ER} being perturbed, leading to autophagy in HCC.

Acknowledgments

This study was supported by the National Natural Science Foundation of China (81973350, China) and Beijing Natural Science Foundation (7222253, China). The study was also supported by the National Natural Science Foundation of China (81872884 and 82173841, China). We thanked Prof. Shuhua Wu (Department of Pathology, Binzhou Medical University Hospital, Shandong, China), for her contribution to providing human liver cancer specimens.

Author contributions

Shuxiang Cui and Xianjun Qu conceived the project. Yanan Li, Keqin Li, Ting Pan, Qiaobo Xie, Yuyao Cheng, Xinfeng Wu, Rui Xu, Xiaohui Liu, Li Liu, Jingming Gao and Wenmin Yuan performed experiments. Shuxiang Cui assured the results. Xianjun Qu performed the statistical analysis and wrote the manuscript. All authors approved the final version of the manuscript.

Conflicts of interest

The authors declare no conflicts of interest.

Appendix A. Supporting information

Supporting data to this article can be found online at https://doi.org/10.1016/j.apsb.2023.05.031.

References

1. Stalnecker CA, Grover KR, Edwards AC, Coleman MF, Yang RY, Deliberty JM, et al. Concurrent inhibition of IGF1R and ERK increases pancreatic cancer sensitivity to autophagy inhibitors. *Cancer Res* 2022;**82**:586−98.
2. Vartanian S, Lee J, Klijn C, Gnad F, Bagniewska M, Schaefer G, et al. ERBB3 and IGF1R signaling are required for Nrf2-dependent growth in KEAP1-mutant lung cancer. *Cancer Res* 2019;**79**:4828−39.
3. Hua H, Kong Q, Yin J, Zhang J, Jiang Y. Insulin-like growth factor receptor signaling in tumorigenesis and drug resistance: a challenge for cancer therapy. *J Hematol Oncol* 2020;**13**:64.
4. Ngo MT, Jeng HY, Kuo YC, Nanda JD, Brahmadhi A, Ling TY, et al. The role of IGF/IGF-1R signaling in hepatocellular carcinomas: stemness-related properties and drug resistance. *Int J Mol Sci* 2021;**22**:1931.
5. Lin SL, Lin CY, Lee W, Teng CF, Jeng LB. Mini review: molecular interpretation of the IGF/IGF-1R axis in cancer treatment and stem cells-based therapy in regenerative medicine. *Int J Mol Sci* 2022;**23**:11781.
6. Wang Q, Zhang Y, Zhu J, Zheng HG, Chen ST, Chen L, et al. IGF-1R inhibition induces MEK phosphorylation to promote survival in colon carcinomas. *Signal Transduct Targeted Ther* 2020;**5**:153.
7. Papp B, Launay S, Gelebart P, Arbabian A, Enyedi A, Brouland JP, et al. Endoplasmic reticulum calcium pumps and tumor cell differentiation. *Int J Mol Sci* 2020;**21**:3351.
8. Aguayo-Ortiz R, Espinoza-Fonseca LM. Linking biochemical and structural states of SERCA: achievements, challenges, and new opportunities. *Int J Mol Sci* 2020;**21**:4146.
9. Molenaar JP, Verhoeven JI, Rodenburg RJ, Kamsteeg EJ, Erasmus CE, Vicart S, et al. Clinical, morphological and genetic characterization of Brody disease: an international study of 40 patients. *Brain* 2020;**143**:452−66.
10. Cui C, Merritt R, Fu L, Pan Z. Targeting calcium signaling in cancer therapy. *Acta Pharm Sin B* 2017;**7**:3−17.
11. Bruce JI, James AD. Targeting the calcium signalling machinery in cancer. *Cancers* 2020;**12**:2351.
12. Huang YL, Shen ZQ, Wu CY, Teng YC, Liao CC, Kao CH, et al. Comparative proteomic profiling reveals a role for Cisd2 in skeletal muscle aging. *Aging Cell* 2018;**17**:e12705.
13. Fan L, Lu C, Fan Y, Tian XY, Lu S, Zhang PF, et al. High-fat diet promotes colorectal carcinogenesis through SERCA2 mediated serine phosphorylation of Annexin A2. *Int J Biochem Cell Biol* 2022;**145**:106192.
14. Chen CC, Chen BR, Wang YN, Curman P, Beilinson HA, Brecht RM, et al. Sarco/endoplasmic reticulum Ca^{2+}-ATPase (SERCA) activity is required for V(D)J recombination. *J Exp Med* 2021;**218**:e20201708.
15. Doan NT, Paulsen ES, Sehgal P, Moller JV, Nissen P, Denmeade SR, et al. Targeting thapsigargin towards tumors. *Steroids* 2015;**97**:2−7.
16. Shin GC, Moon SU, Kang HS, Choi HS, Han HD, Kim KH. PRKCSH contributes to tumorigenesis by selective boosting of IRE1 signaling pathway. *Nat Commun* 2019;**10**:3185.
17. Ibarra C, Vicencio JM, Estrada M, Lin Yb, Rocco P, Munoz JP, et al. Local control of nuclear calcium signaling in cardiac myocytes by perinuclear microdomains of sarcolemmal insulin-like growth factor 1 receptors. *Circ Res* 2013;**112**:236−45.
18. Cai B, Zhao J, Zhang YL, Liu YX, Ma CH, Yi F, et al. USP5 attenuates NLRP3 inflammasome activation by promoting autophagic degradation of NLRP3. *Autophagy* 2022;**18**:990−1004.
19. Granatiero V, Sayles NM, Savino AM, Konrad C, Kharas MG, Kawamata H, et al. Modulation of the IGF1R−MTOR pathway attenuates motor neuron toxicity of human ALS SOD1G93A astrocytes. *Autophagy* 2021;**17**:4029−42.
20. Cai B, Ma M, Zhang J, Wang ZJ, Kong SF, Zhou Z, et al. LncEDCH1 improves mitochondrial function to reduce muscle atrophy by interacting with SERCA2. *Mol Ther Nucleic Acids* 2022;**27**:319−34.
21. Barajaa MA, Nair LS, Laurencin CT. Robust phenotypic maintenance of limb cells during heterogeneous culture in a physiologically relevant polymeric-based constructed graft system. *Sci Rep* 2020;**10**:11739.
22. Zhang Z, Qian Q, Li M, Shao F, Ding WX, Lira VA, et al. The unfolded protein response regulates hepatic autophagy by sXBP1-mediated activation of TFEB. *Autophagy* 2021;**17**:1841−55.
23. Xiu M, Huan X, Ou Y, Ying S, Wang JM. The basic route of nuclear-targeted transport of IGF-1/IGF-1R and potential biological functions in intestinal epithelial cells. *Cell Prolif* 2021;**54**:e13030.
24. Shenoy SK, Lefkowitz RJ. β-Arrestin-mediated receptor trafficking and signal transduction. *Trends Pharmacol Sci* 2011;**32**:521−33.
25. Aleksic T, Gray N, Wu X, Rieunier G, Osher E, Mills J, et al. Nuclear IGF1R interacts with regulatory regions of chromatin to promote RNA polymerase II recruitment and gene expression associated with advanced tumor stage. *Cancer Res* 2018;**78**:3497−509.
26. Centonze FG, Reiterer V, Nalbach K, Saito K, Pawlowski K, Behrends C, et al. LTK is an ER-resident receptor tyrosine kinase that regulates secretion. *J Cell Biol* 2019;**218**:2470−80.
27. Yin Y, Hua H, Li M, Liu S, Kong QB, Shao T, et al. mTORC2 promotes type I insulin-like growth factor receptor and insulin receptor activation through the tyrosine kinase activity of mTOR. *Cell Res* 2016;**26**:46−65.
28. Wei X, Zheng ZY, Feng ZH, Zheng L, Tao SY, Zheng BJ, et al. Sigma-1 receptor attenuates osteoclastogenesis by promoting ER-associated degradation of SERCA2. *EMBO Mol Med* 2022;**14**:e15373.

29. Quan C, Li M, Du Q, Chen QL, Wang H, Campbell D, et al. SPEG controls calcium reuptake into the sarcoplasmic reticulum through regulating SERCA2a by its second kinase-domain. *Circ Res* 2019;**124**: 712−26.
30. Rossi AM, Taylor CW. Reliable measurement of free Ca^{2+} concentrations in the ER lumen using Mag-Fluo-4. *Cell Calcium* 2020;**87**: 102188.
31. Dries E, Santiago DJ, Gilbert G, Lenaerts I, Vandenberk B, Nagaraju CK, et al. Hyperactive ryanodine receptors in human heart failure and ischaemic cardiomyopathy reside outside of couplons. *Cardiovasc Res* 2018;**114**:1512−24.
32. Preissler S, Rato C, Yan Y, Perera L, Czako A, Ron D, et al. Calcium depletion challenges endoplasmic reticulum proteostasis by destabilising BiP-substrate complexes. *Elife* 2020;**9**:e62601.
33. Ngo MH, Jeng HY, Kuo YC, Nanda JD, Brahmadhi A, Ling TY, et al. The role of IGF/IGF-1R signaling in hepatocellular carcinomas: stemness-related properties and drug resistance. *Int J Mol Sci* 2021;**22**:1931.
34. Werner H, Sarfstein R, LeRoith D, Bruchim I. Insulin-like growth factor 1 signaling axis meets p53 genome protection pathways. *Front Oncol* 2016;**6**:159.
35. Xue N, Lai FF, Du TT, Ji M, Liu D, Yan CH, et al. Chaperone-mediated autophagy degradation of IGF-1Rβ induced by NVP-AUY922 in pancreatic cancer. *Cell Mol Life Sci* 2019;**76**:3433−47.
36. Crudden C, Shibano T, Song D, Dragomir MP, Cismas S, Serly J, et al. Inhibition of G protein-coupled receptor kinase 2 promotes unbiased downregulation of IGF1 receptor and restrains malignant cell growth. *Cancer Res* 2021;**81**:501−14.
37. Shintani Y, Hayata-Takano A, Moriguchi K, Nakazawa T, Ago Y, Kasai A, et al. β-Arrestin1 and 2 differentially regulate PACAP-induced PAC1 receptor signaling and trafficking. *PLoS One* 2018;**13**: e0196946.
38. Aamna B, Dan AK, Sahu R, Behera SK, Parida S. Deciphering the signaling mechanisms of β-arrestin1 and β-arrestin2 in regulation of cancer cell cycle and metastasis. *J Cell Physiol* 2022;**237**:3717−33.
39. Jha A, Chung WY, Vachel L, Maleth J, Lake S, Zhang GF, et al. Anoctamin 8 tethers endoplasmic reticulum and plasma membrane for assembly of Ca^{2+} signaling complexes at the ER/PM compartment. *EMBO J* 2019;**38**:e101452.
40. Fan MM, Gao J, Zhou L, Xue WW, Wang YX, Chen JW, et al. Highly expressed SERCA2 triggers tumor cell autophagy and is a druggable vulnerability in triple-negative breast cancer. *Acta Pharm Sin B* 2022; **12**:4407−23.
41. Marchi S, Giorgi C, Galluzzi L, Pinton P. Ca^{2+} fluxes and cancer. *Mol Cell* 2020;**78**:1055−69.
42. Foerster EG, Mukherjee T, Cabral-Fernandes L, Rocha JD, Girardin SE, Philpott DJ. How autophagy controls the intestinal epithelial barrier. *Autophagy* 2022;**18**:86−103.
43. Beauvais DM, Jung O, Yang Y, Sanderson RD, Rapraeger AC. Syndecan-1 (CD138) suppresses apoptosis in multiple myeloma by activating IGF1 receptor: prevention by synstatinIGF1R inhibits tumor growth. *Cancer Res* 2016;**76**:4981−93.
44. Piao WH, Wang Y, Adachi Y, Yamamoto H, Li R, Imsumran A, et al. Insulin-like growth factor-I receptor blockade by a specific tyrosine kinase inhibitor for human gastrointestinal carcinomas. *Mol Cancer Therapeut* 2008;**7**:1483−93.
45. Pagliaro L, Marchesini M, Roti G. Targeting oncogenic Notch signaling with SERCA inhibitors. *J Hematol Oncol* 2021; **14**:8.